

THE PENNSYLVANIA STATE UNIVERSITY  
SCHREYER HONORS COLLEGE

DEPARTMENT OF MECHANICAL ENGINEERING

Defect Identification and Classification of Cellular Glass

BENJAMIN BURLOVIC  
SPRING 2023

A thesis  
submitted in partial fulfillment  
of the requirements  
for baccalaureate degrees  
in Mechanical Engineering and Economics  
with honors in Mechanical Engineering

Reviewed and approved\* by the following:

Dr. Ryan Harne  
Associate Professor of Mechanical Engineering  
Thesis Supervisor

Dr. Margaret Byron  
Assistant Professor of Mechanical Engineering  
Honors Adviser

\* Electronic approvals are on file.

## ABSTRACT

Cellular glasses are heavily employed insulation materials due to their high strength-to-weight ratio, low cost in mass production, closed-cell microstructure, and low conductivity. The high strength-to-weight ratio stems from the porous microstructure of cellular glass. The porosity of cellular glass is characterized by millions of thin glass-walled cells filled with pressurized gasses (CO<sub>2</sub> and O<sub>2</sub>). When compressed, these cells absorb high amounts of pressure while maintaining a low density and subsequent weight. The size and distribution of the cells drive the compressive strength of a given cellular glass sample and can range from 1.5 – 5 MPa. The high variation in strength leads to the failure of products when operating under normal conditions. A major challenge faced by manufacturers of cellular glass is the lack of a non-destructive testing (NDT) method. They can't analyze an entire sample's microstructure without cutting into the block and visually inspecting the cells. This research seeks to undertake a series of exhaustive computational designs and experimentation to investigate how the true material properties of a given cellular glass sample can be identified. Specifically, the use of a neural network to perform defect detection using computerized tomography scans of cellular glass is explored. A logistical regression neural network for image classification was designed and written in the MATLAB platform and tested for its accuracy and efficiency. The results showed the neural network was highly accurate, with a peak rating of 100%, and efficient with a variety of sample data. The results of this research will guide future work to create an independent operating NDT system to characterize cellular glass products during the manufacturing of products and ultimately limit failures in the field.

## TABLE OF CONTENTS

LIST OF FIGURES .....	iii
LIST OF TABLES .....	iv
ACKNOWLEDGEMENTS .....	v
Chapter 1 Introduction .....	1
Defect Detection in Porous Materials .....	2
Classification of Porous Materials .....	3
Image Classification Neural Networks of Structural Materials .....	5
Cellular Glass .....	6
Objective .....	8
Chapter 2 Methodology .....	9
2.1 Data Acquisition .....	9
2.2 Data Upload and Processing .....	12
2.3 Description of Neural Network Architecture .....	13
2.4 Experimental Setup .....	16
Chapter 3 Results and Discussions .....	17
3.1 Baseline Code Performance .....	17
3.2 Expansion of Sample Size .....	19
3.3 Investigation of Resizing Scans .....	21
3.4 Investigation of Rotating Images .....	22
3.5 Summary of Results .....	26
Chapter 4 Conclusions .....	28
Appendix A .....	33

**LIST OF FIGURES**

Figure 1. Fitting Diagram .....	6
Figure 2. Cut Block of Cellular Glass .....	10
Figure 3. Wrapped Sample of Cellular Glass .....	10
Figure 4: Healthy (left) and Defective (right) Sample Scans .....	11
Figure 5. Example Scans at Varying Angles .....	13
Figure 6. Neural Network Architecture .....	14
Figure 7. Sigmoid Function .....	15
Figure 8. (Left to Right) Defective Sample and Healthy Sample Before and After Modified Aspect Ratios .....	21
Figure 9. Artificial Defect Sample by Rotation .....	23
Figure 10. Idealized Illustration of the Model Applied to Rotated Scans .....	25

**LIST OF TABLES**

Table 1. Baseline Results.....	18
Table 2. Sample Size Expansion Results.....	20
Table 3 Aspect Ratio Results.....	22
Table 4. Rotation Results.....	24
Table 5. Regularization Testing with Rotated Images.....	24

## ACKNOWLEDGEMENTS

I would like to start by saying thank you to my thesis supervisor Dr. Harne for being an amazing resource and leader during my final two years at Penn State. I am grateful that he took me in as an undergraduate researcher in the Laboratory of Sound and Vibrations Research the following semester.

Next, I'd like to thank Dr. Byron, my honors advisor and faculty reader.

Additionally, I want to thank Owens Corning for providing the LSVR team with samples of cellular glass for our testing. This thesis would not have been possible without their commitment and contribution.

Thank you to the Schreyer Honors College staff, many of who I've had the pleasure of working alongside in various positions and clubs. The honors college will forever hold a special place in my heart and I'm lucky to have been a part of it.

Without further ado, I'd like to thank my parents and younger brother for all their support throughout my four years at Penn State. They have been a consistent rock in my life to lean on when things got hard, and I couldn't be more thankful for them.

## **Chapter 1**

### **Introduction**

Cellular glass is an insulation material with unique characteristics that meet high-stress engineering projects. Applications of the material span from commercial/residential uses like roofing and flooring to industrial projects like oil rig foundations and process piping [1], [2]. Its most notable attributes are that it is impervious to moisture, inert, and has high compressive strength [3], [4]. A major challenge faced by cellular glass manufacturers is a lack of nondestructive testing (NDT) for defect detection. Currently, the only methods of finding defects are limited to destructive and electronic probe analysis both of which are costly and inefficient [5].

This ultimately has led manufacturers to unknowingly send faulty products to customers which are at a higher risk of crack propagation and failure when placed under normal operating conditions. The goal of this thesis is to prove the concept of creating a machine learning tool to accurately identify defective samples of cellular glass using computed tomography (CT) scans. The first step toward proof of concept is to explore existing literature on NDT methods of porous materials with similar microstructures as cellular glass. Second, a suitable machine learning architecture for analysis of the high-definition images resultant of CT imagery will be designed and created. Next, stress testing of the model with CT scans of the sample cellular glass will be completed. Finally, the results will be analyzed to determine the viability of creating an image classification AI to perform defect identification and classification on basic cellular glass.

## Defect Detection in Porous Materials

To create a non-destructive defect detection system for cellular glass, evidence of similar techniques on porous materials must be strong. Porous materials pose a unique challenge when imaging due to their lack of uniformity and varying densities [6], [7].

Concrete and other cementitious material are heavily researched and tested porous materials, with crack propagation similar to cellular glass [8], [9]. Concrete is a composite material made of aggregates that are bonded by a cement paste, like the glass powder and bonding agent used in cellular glass [4]. Research investigated the use of Ultrasonic Wave Reflection (UWR) to characterize early-age concrete and cementitious material. While there are many variations in the set-up of testing configurations, there is uniformity in the core elements: transducers to send and receive the signal, wave type produced by the transducers, and a buffer material between the transducers and sample [9]. Unique wave types and corresponding frequency and buffer materials were needed to test the samples as they aged. Research on UWR applicability on concrete concluded with findings of large flexibility across the aging process of concrete, mortar, and cementitious materials. While findings support the use of NDT on concrete and other cementitious materials, similar success with homogenous materials will further support the case for the use of ultrasonics of cellular glass [9].

Steel is another material that has been a subject of NDT testing research, with a major focus on separating diffracted ultrasonic signals from noise [10]. This issue becomes especially large when the area of interest (a crack) is rather small in comparison to the rest of the image. To circumvent this, image formation was avoided and instead sparse matrix elements were created to form a decision boundary [10]. An additional benefit of using sparse matrix analysis over image formation is the lowered demand for data storage. Full image formation becomes a burden

on one's hard drive and can be a detriment to the speed at which analysis can be performed. The final step was applying the Hough Transform algorithm designed to detect the hyperbolas, indicating cracks in the microstructure of the test steel. These results improved the performance of ultrasonic testing both in terms of speed and success rate. The success in applying ultrasonic testing on steels proves valuable and supplements the research on concrete and cementitious materials. However, steel is not as strong of a benchmark material to cellular glass as cement and cementitious materials. Still, the noise reduction and data efficiency challenges with steel samples faced are shared by cellular glass. Altogether, both references [9] and [10] showed compelling evidence that ultrasonic imagery could be applied as a non-destructive defect detection for cellular glass.

### **Classification of Porous Materials**

Following the evidence of non-destructive defect detection methods with porous materials, it is critical to assess the implementation of ultrasonic scans into image classification software. In supervised image classification algorithms, a set of sample data is inputted along with associated classifier(s). The goal of the algorithm is to create a graphical boundary separating "good" data from "bad." At a high level, the algorithm creates a regression function capable of predicting the identity of a given image based on the data from the initial test set. In the case of complicated imagery like in CT scans [7], neural networks are needed to complete the analysis. An image classification neural network simultaneously performs the regression outlined above across several nodes which are repeated across many layers. The interaction between the nodes in

neural networks allows for the image to be broken down and ultimately allows for accurate interpretation.

Additively manufactured parts face the constant challenge of varying conditions that lead to defects in their structural integrity [11]. Their porous microstructure makes for a strong benchmark for cellular glass. Research set out to determine if direct laser deposition scans of part melt pools could predict abnormalities in the microstructure of the final part. To achieve this, the scans measured simple metrics of the melt pool such as length, width, temperature, etc. [11].

Multiple supervised learning classification methods were tested including Decision Tree (DT), K-Nearest Neighbor (KNN), Support Vector Machine (SVM), and Discriminant Analysis (DA) [11]. Decision Tree classification models work by recursive splitting of the input data into subsets based on their values until they match with an output label. K-Nearest Neighbor models make hypotheses of new samples based on their similarity to the K-closest test data points.

Support Vector Machine classification makes hypotheses of new data using a planar boundary to separate various classes.

Ultrasonic imagery has improved the classification of deep-partial thickness burns, which are the most difficult to identify; traditional methods only record an accuracy of ~80% [12]. Using a multiclass deep convolutional neural network (CNN) architecture in the classification of burn depths has achieved 95% accuracy [12]. While the success of CNN architecture supplements the findings on additive manufacturing, it must be stated that the similarities between medical and manufacturing samples are limited. However, the data collected by ultrasonic devices are similar and both sources concluded with high accuracy levels. Consequently, compelling evidence exists to suggest that imagery data of cellular glass can be accurately analyzed by an image classification algorithm to detect defects.

## Image Classification Neural Networks of Structural Materials

When performing image classification, data sizes can grow exponentially. Neural networks are used to make non-linear hypotheses, allowing for software to perform the more advanced functions required. Neural networks are comprised of multiple layers of interconnected nodes that hold onto information that is then passed on to the other nodes in the network. The input/first layer of a neural network receives the initial data which is then passed through a series of hidden layers of nodes. As the data is passed through the hidden layers, each performs a transformation based on its assigned weight. The final or output layer produces the model's predictions. Neural networks are trained using a test data set that has both the raw data and its identity. During training, the network adjusts the weights and biases of its nodes to reduce the difference between its predictions and the true values. This is done using optimization algorithms, such as gradient descent, which iteratively adjusts the weights and biases to reduce the error between the predicted output and the true output.

Image classification neural networks have success in accurately predicting and classifying structural materials [5]–[7], [13]–[15]. Models can be uniquely designed to meet the needs and challenges of the images they are trained on and predicting. Trained models can predict the material properties of a sample as quickly as one second without the need for a strong computing system [15]. However, an issue that can arise in these models is the overfitting of the test data, which occurs when the decision model does not generalize and fits too closely to the training set. Figure 1 shows a visual of overfitting in a two-dimensional training set. As shown in the overfitting example, the model (represented by the line) factors in outliers and risks

misclassifying images outside of the training set. Instead, the model should take a more generalized approach as shown in the optimal fitting example to ensure accurate predictions.

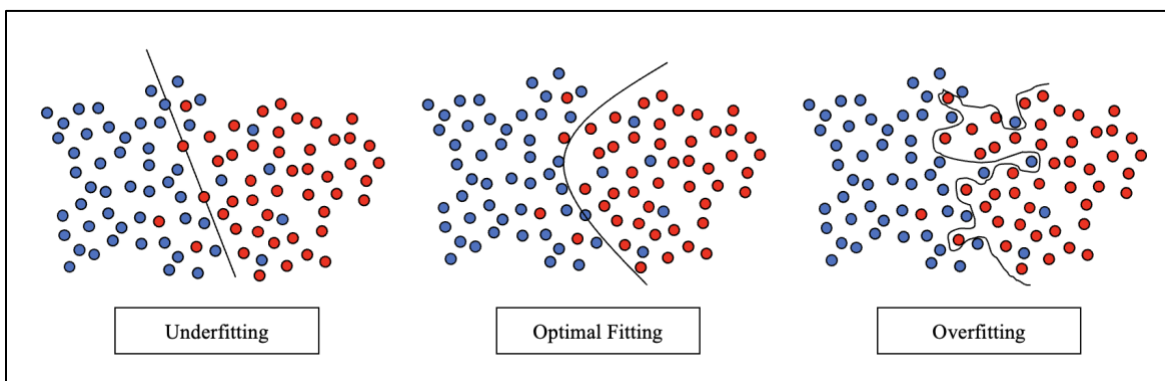


**Figure 1. Fitting Diagram**

Regularized neural networks (RNNs) can be used to add noisiness or penalties to the model to prevent overfitting and approach an optimal fit [14]. The process of fitting a model via regularization is iterative and can take many forms. A common method is to apply a penalty term to the optimization algorithms used to calculate the weights of the nodes [13]–[16].

### **Cellular Glass**

Cellular glass is an industrial material regarded for its high compressive strength, low thermal conductivity, and closed-cell structure. Because it is entirely made of glass, the material is non-combustible allowing for use in extreme temperature conditions [4], [17]. Its market includes but is not limited to architectures: (floor insulation, plaza insulation), industrials: (below and above ground piping, floating tank insulation, tank/equipment bases), and specialties (abrasives, heat exchanger surface) [1], [3], [4]. The major challenge manufacturers face stems from the variation

in the production of cellular glass that leads to inconsistent material properties and in some cases terminal defects.

The raw materials of cellular glass can be simplified down to a recycled glass powder and its foaming agent. Additionally, cellular glass is a hetero-phase material meaning that it simultaneously contains both solid and gaseous phases [3]. During formation, micrometer-thick walls take shape enclosing gas-filled bubbles resulting in high porosity and subsequent high compressive strength [4]. Research found that large cells formed when the foaming agent content grew [4]. Additionally, decreasing the size of the glass powder particles leads to a lower uniformity across the microstructure [4]. The categories of the powder distribution in the research can be broken down into L1 (coarse pores > fine pores), L2 (coarse pores = fine pores), and L3 (coarse pores < fine pores) [4]. Moreover, the distribution of the foaming content ranged from one to two percent by weight. Across the testing variations, the observed effects on samples' densities varied from none to significant. The result of the variation in density played a large role in affecting the material properties [18].

The key trait of cellular glass, its compressive strength, is derived from its high level of porosity [1]. The porosity of a sample varied greatly when minor changes were made to the inputs of the manufacturing process. This leads to a high variation in density (120 – 400 kg/m<sup>3</sup>) and strength (1.5 – 5 MPa) [4]. A major challenge faced by manufacturers is identifying samples whose material properties fall outside a standard uncertainty and are at risk of failure.

The inability to perform reliable defect detection becomes a major manufacturing challenge when cellular glass is produced at scale and the variation in cooling conditions is increased. Currently, manufacturers are hearing from clients that some cellular glass blocks exhibit cracking and in extreme cases total failure when under normal operating conditions. Fortunately,

preliminary testing has shown that CT scans of cellular glass could be performed fast and effectively. This finding led to the possibility of using an image classification algorithm to accurately identify defective samples.

### **Objective**

As discussed above, past work has shown that an array of methods to process imagery data of material exist, each chosen to match the challenges of their test material. High efficiency and accuracy have been reached in the image classification of various porous materials. While these investigations show promise in NDT of materials similar to cellular glass, this research will explore the effectiveness of a regularized neural network in performing defect identification and classification on cellular glasses. By designing a distinct RNN tailored to the features of CT scans of cellular glass, testing will be completed to find the limitations of the model. Finding where the model fails will significantly improve the understanding of cellular glass defects. It will provide the foundation for creating an independent NDT system for manufacturers to achieve lower failure rates of their products.

## **Chapter 2**

### **Methodology**

This research includes both data acquisition and computational studies to fully comprehend the feasibility of defect identification and classification of cellular glass. Therefore, this chapter will introduce the computerized tomography of the cellular glass samples, the creation of artificial defects, and the performed processing of the scans. Furthermore, the regularized neural network design and experimental setup will be described.

#### **2.1 Data Acquisition**

The CT scans used in this research were performed by Sara Mueller at the Center for Quantitative Image (CQI) at the Pennsylvania State University, for the Laboratory of Sound and Vibration Research (LSVR). Each scan produced approximately one-thousand unique tiff images ranging from 3.5 – 5 million total pixels. The scans were produced by rotating the glass sample about its vertical axis to obtain scans at varying angles.

The LSVR's inventory of cellular glass samples needed to be cut down into smaller blocks for the CT equipment at the CQI. The abundant flaking of cellular glass when handled posed a health hazard for members of the lab and proper PPE and safe practices needed to be put into place. Two individuals were required to cut a sample of the glass: one to perform the cutting using a sharpened knife and another to hold a vacuum close to the cut site to limit the glass flakes from spreading. Both individuals wore medical gloves underneath coated fabric gloves and a disposable mask. A sample block is shown in Figure 2.

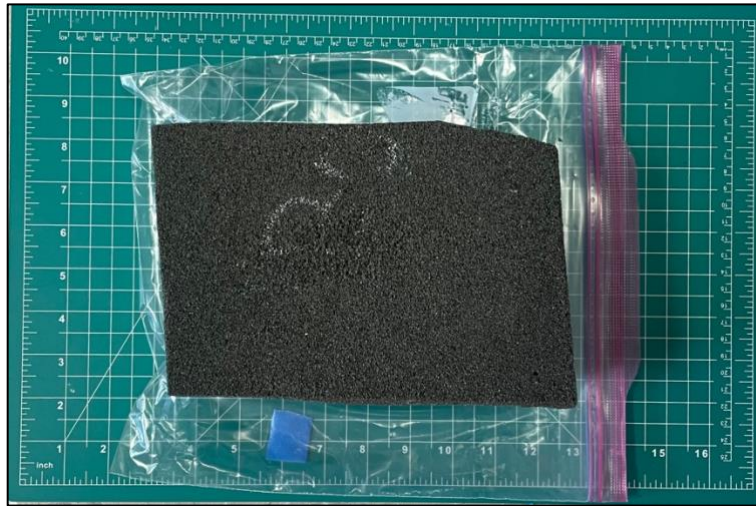


**Figure 2. Cut Block of Cellular Glass**

After a sample was cut, it was carefully wrapped in paper towels followed by plastic wrap to reduce the risk of glass dust from spreading during the transport and imaging of each sample as shown in Figure 3.



**Figure 3. Wrapped Sample of Cellular Glass**

The first eight samples scanned all returned what appeared to be perfectly “healthy” images, having no cracks and uniform porosity. The decision was made to artificially create a defective sample from a previously scanned block to have a clear comparison for the neural network and cut imaging costs. To produce the defective sample, the prior block was carefully removed from

its wrapping with a vacuum to remove any new glass dust. Then a screwdriver and knife were used to simulate cracks and air pockets in the sample. A side-by-side comparison of the block before and after the defect creation is shown in Figure 4. In the top right corner of the defective scan, two hollowed areas simulating defects are shown (designated by red circles). The top one was created by driving a screwdriver into the side of the sample of cellular glass to mimic cavities in cellular glass. Below that is a smaller hole created by driving a knife into the side of the sample to mimic a crack in a block of cellular glass.

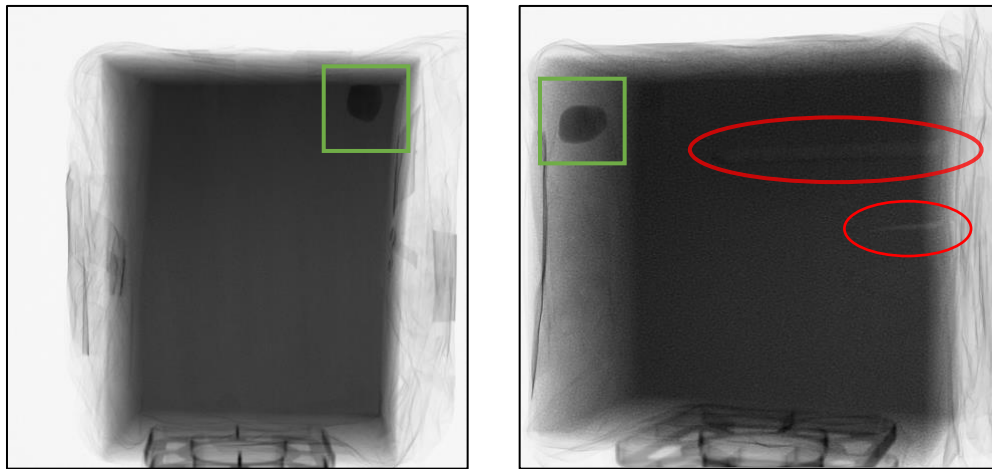


**Figure 4: Healthy (left) and Defective (right) Sample Scans**

Each scan includes irrelevant data to the microstructure of its sample of cellular glass. This includes the wrapping surrounding the blocks, the base plate at the bottom of the blocks, and the orientation marker in the top right and left corners (designated by green boxes). These features of the scan hold no significance, and will not make an impact on the accuracy of the neural network because they will be factored into the model. All the sample scans include imagery of the wrapping, base plate, and marker, so the irrelevant data will not make any impact on the neural network decision boundary.

## 2.2 Data Upload and Processing

The CT scans were uploaded, processed, and saved in MATLAB for use in the neural network. We note that the scans of the healthy and defective samples were different sizes (2014-by-2024 pixels for the healthy and 2014-by-1900 pixels for the defective). The neural network used in this research performs its calculations via matrix operations, requiring the sizes of the matrices to be the same. To achieve the same data size for each sample, the white space above and a portion of the base plate below the unhealthy scans were cropped so that their matrices were 2014-by-1900 pixels. Cropping of the healthy image was performed out of necessity as the healthy scans were taken at different parameters resulting in the differing sizes. It was assumed that because the defects were still shown in the sample data along with some of the noise features (base plate and wrapping). The validity of this assumption is reported in the first testing reports.

After matching the scans' sizes, further processing of the data was necessary as the neural network used in this research utilizes vectorization to achieve higher levels of efficiency. Therefore, the images were unwrapped into vectors and converted from uint16 to doubles. Finally, a second vector was saved to hold the labels of each scan and complete the test data upload and preparation. The chosen labels were the digits "1" and "2" corresponding to defective and healthy samples respectively. Note that MATLAB does not have a zero index and choosing "0" to be a label will lead to incorrect predictions. Note if two scans resulted in a different number of pixels then the larger must be cropped to be the same size as the smallest to perform the matrix operations in the neural network, as discussed above.

The large number of pixels for a given image meant that the total number of samples in test data was initially limited to have an efficient code run time. Therefore, the initial sample set was composed of 200 total CT scans: 10 defective and 190 healthy. Careful selection of the scans for

the sample was taken to have a varying array of angles as shown in Figure 5. Applying a diverse selection of scans was crucial to properly test the code as it allowed for what was one defective sample to be translated into many different ones.

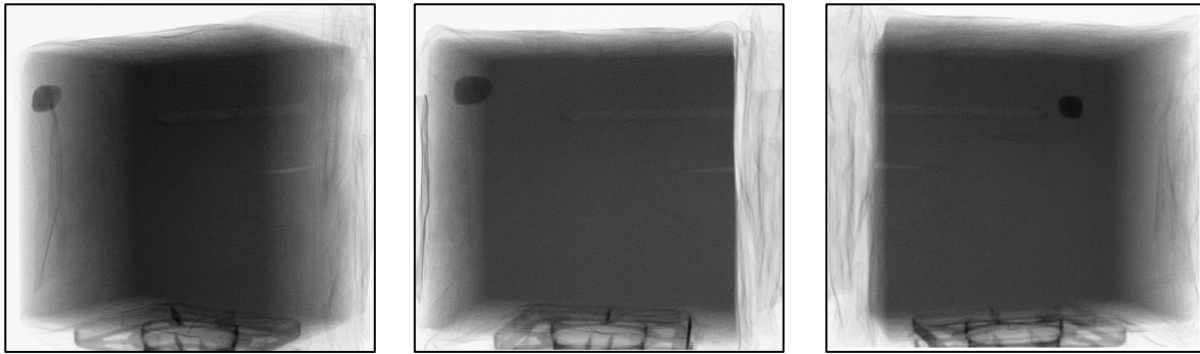


**Figure 5. Example Scans at Varying Angles**

### **2.3 Description of Neural Network Architecture**

The architecture design for this thesis is a three-layer regularized logistical regression neural network using the pixel data from CT scans as the input. As stated, the input layer of the neural network is comprised of individual nodes equaling to the total number of pixels in the test scan with each node holding the numeric value for a given pixel. The hidden layer was comprised of twenty-five nodes that contained the transformed data from the input layer. Finally, the data held in the second layer was used to calculate the hypothesis in the final layer made up of two nodes corresponding to either a healthy or defective sample prediction. Figure 6 shows a visual representation of the neural network and how it interacts to generate predictions.

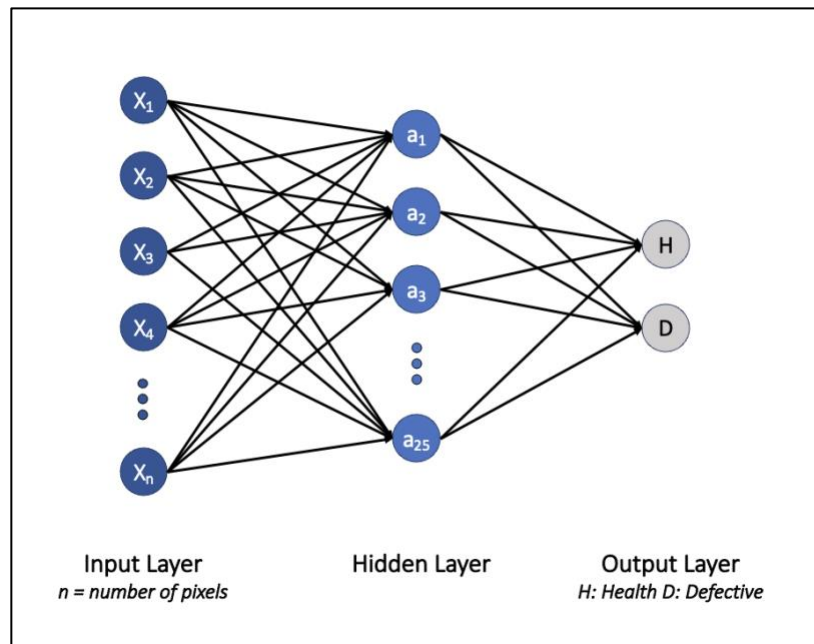


**Figure 6. Neural Network Architecture**

To train the neural network the first step was to randomly initialize the weights that the transformations of the input data and the hidden layer were based on. The randomly initialized weights were stored in matrices, called theta, with the number of rows equal to the size of the input layer and the number of columns equal to the number of nodes in the hidden layer. For example, the first initial theta was a 3826600-by-25 matrix corresponding to the number of pixels in the scans and the number of nodes in the hidden layer. Next, feedforward propagation takes place and calculates a hypothesis for each image used in the training set. Feedforward propagation is the process of working through the neural network as designed: the input data is transformed via a sigmoid function (logistic function) using the randomized weights culminating in a prediction of the data set in the output layer. By applying a sigmoid function as the transformation, the hypothesis can be bounded to our chosen variables. Fig. 7 shows the sigmoid function used in this network along with a graphical representation depicting how it can be bounded to a range of  $[0,1]$ . In this case, the variable  $x$  corresponds to theta.

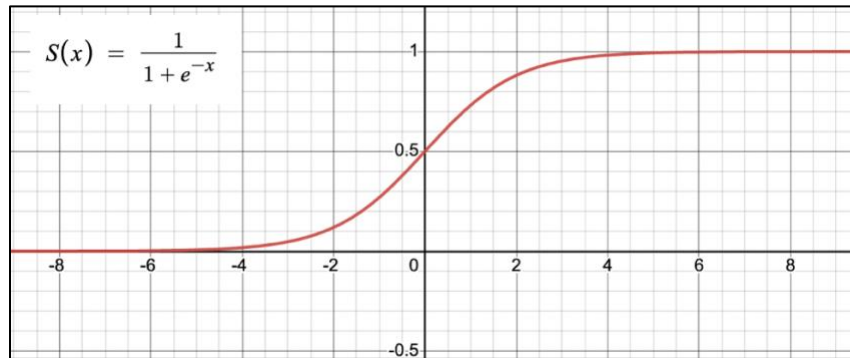


**Figure 7. Sigmoid Function**

Following feedforward propagation, a cost function is calculated using the calculated hypothesis. A cost function is a measurement of the error rate of feedforward propagation. It calculates the difference between the hypothesis and the true value of the test data. The next step is to implement backpropagation which minimizes the cost function (difference in predicted and true values) via a gradient descent function. The backpropagation in this neural network works by factoring in the cost function to fine-tune the theta parameters. Gradient descent is an iterative optimization algorithm that finds the local minimum of a given function which is the cost function in the case of this research. The final step in training the neural network was to apply regularization to the thetas in the form of weight penalization. The weight penalty, lambda, curbs the overfitting of the model by increasing the weight of terms in the neural network by increasing their cost. Therefore a larger lambda will increase the weights than a lower one causing a smoother or more generalized model fit. The front-end code and all relevant functions can be referenced in Appendix A. The value of the penalty was tuned throughout the testing process and is reported in Chapter 4. With properly tuned weights to transform the data from the input to the output layer, the neural network was ready to identify and classify samples of cellular glass.

## 2.4 Experimental Setup

After the scan data was acquired, uploaded, processed, and the neural network written, a baseline set of parameters with varying training set sizes and regularization penalties was tested. Using those results, further testing was completed to determine what caused the model to fail.

Throughout these tests, the randomly initialized theta matrices were held constant at the beginning of each training test to prevent undue variation in the efficiencies and accuracies. First, the sample size was incrementally increased while keeping the training set size constant. Second, a possible solution to the mismatched scan sizes was explored by adjusting the aspect ratios of each scan during the processing step. Finally, scans outside of the training set were rotated during the processing step to simulate new defects and challenge the model.

## Chapter 3

### Results and Discussions

From the experimental data gained from the series of testing on the neural network, the results were analyzed to investigate the accuracy, efficiency, and failure characteristics of the model. Observations of the model failure yield greater insight into the application of this neural network at larger scales. Manipulations of the scans to improve efficiency and accuracy are also investigated. Finally, the artificial creation of new defective samples is explored to add increased variation to the data set.

#### 3.1 Baseline Code Performance

As mentioned in section 2.4, a baseline set of parameters was chosen for the neural network for initial testing and tuning. The chosen architecture was composed of one hidden layer containing 25 nodes, the regularization factor  $\lambda$  set to 1.0, and 40 training iterations. The number of training iterations was set to 20% to have a significant amount of images not included in the weight calculation to better test the model fit. The data set was a total of 200 CT scans comprised of 10 defective and 190 healthy samples. The reported accuracy was 100%, with a run-time of approximately 546 seconds. Following this result, tests were completed with varying regularization ( $\lambda$ ) values to test for which images would be misclassified when the model was generalized. Additionally, the training iterations were lowered to gain insight into possible heightened efficiencies. All other variables were kept constant including the initial theta matrices

which were only randomly initialized once. Table 1 shows the reported accuracies and run time for each specification.

**Table 1. Baseline Results**

<b>TEST METHOD</b>	<b>REPORTED ACCURACY (PREDICTION = LABEL)</b>	<b>PERFORMANCE (TRAINING TIME)</b>
Baseline	100%	546 sec
<i>Lambda Values</i>		
5	100%	625 sec
20	100%	567 sec
25	100%	594 sec
26	95%	576 sec
27.5	95%	613 sec
30	95%	608 sec
<i>Training Iterations</i>		
30	100%	390 sec
25	95%	324 sec
20	95%	259 sec

Note that the reported accuracy can be misleading: tests that reported 95% accuracy are misclassifying all the defective samples in this data set. The regularization penalty tests concluded that the defective and healthy samples were mutually exclusive. This conclusion was made because there were no lambda values that resulted in a gross accuracy that fell between 95-100%. Furthermore, all the results from the tests on training iterations that resulting in either a perfect classification of defects or none.

The results signified that the model was very strong at classification when tested on the 200-sample set composed of 10 defective and 190 healthy samples. The lack of misclassification of only a portion of the defective samples indicates that the defective data samples are statistically significant from all the healthy ones. Additionally, when the training iteration tests fell below 30, the misclassification was driven by a lack of defective test sets since only 10 were included in the overall sample size. In conclusion, this testing proved the viability of the neural network when used on a small, clean data set and requires additional testing with higher variation in the data to identify any weaknesses.

### **3.2 Expansion of Sample Size**

Building on the results of the baseline testing, the sample size was increased to introduce more variety in defective samples to investigate when the model would misclassify a subset of defective samples rather than all of them. The total sample size was incrementally increased through the addition of samples taken from different angles and was only trained once using a training set of 40 iterations on the first test using 400 samples. The training took approximately twenty minutes. Additionally, the ratio of defective to healthy samples was kept the same as in the preliminary tests. Table 2 reports the results of the increased sample size testing.

**Table 2. Sample Size Expansion Results**

<b>SAMPLE SIZE</b>	<b>REPORTED ACCURACY (PREDICTION = LABEL)</b>
400	<i>100%</i>
800	<i>100%</i>
1200	<i>100%</i>
1600	<i>100%</i>
2000	<i>100%</i>
4000	<i>100%</i>

The results supported the findings in 3.1, which stated that the current defective samples being applied to the neural network are completely mutually exclusive to the healthy samples.

Misclassification would still only occur on the entire set of defective data as was seen in the test done in 3.1.

This testing built on those results by introducing a larger variation in the defective samples through the addition of new, unique angled scans. A limitation of these results is that the cropping of the healthy scans resulted in eliminating some noise elements: wrapping, white space, and the base plate. The next steps in stress testing the model were to test new methods of preprocessing the scans and creating more defective samples and testing them without being included in the test data. In the scope of this research, further defects were artificially created by rotating the existing defective sample in the preprocessing step.

### 3.3 Investigation of Resizing Scans

Building off the results in 3.2, the first step in the testing of rotated scans was to resize the sample matrices to be square. Therefore, before testing rotations, an investigation was completed on changing the aspect ratios of the sample to 1:1. The testing was extended to matching the size of both scans' data sets to evaluate another solution other than cropping. Each scan was resized in the preprocessing section of the code to be 1900-by-1900 pixels. This allowed for the scans to retain the majority of their resolutions and be saved as square matrices which become important in the testing of the neural network. Fig. 8 shows a comparison of defective and healthy scans before and after their aspect ratios were altered. In the defective sample, the screwdriver-induced cavity and incisions from the knife were still clearly visible, and no noticeable changes were seen in the healthy scan.

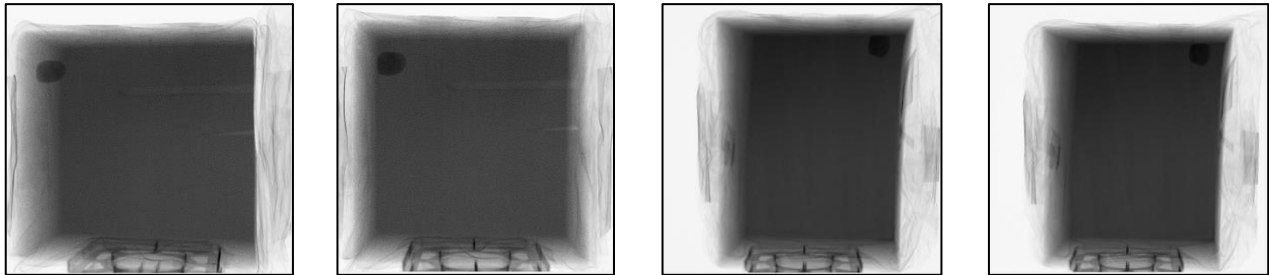


**Figure 8. (Left to Right) Defective Sample and Healthy Sample Before and After Modified Aspect Ratios**

The testing of the altered scans was completed similarly to the sample size expansion testing; with only one round of training on a sample size of 200 followed by an incremental increase in samples.

**Table 3 Aspect Ratio Results**

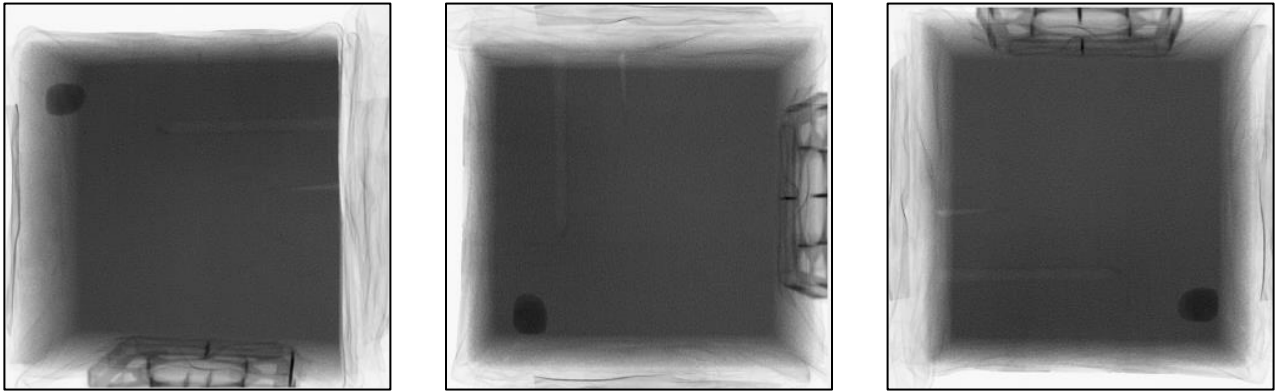
<b>SAMPLE SIZE</b>	<b>REPORTED ACCURACY (PREDICTION = LABEL)</b>
200	<i>100%</i>
400	<i>100%</i>
800	<i>100%</i>
2,000	<i>100%</i>

Table 3 reports the performance of the neural network using the resized scans. The model retained 100% accuracy with the resized images, concluding that the data sets could be resized allowing for a superior preprocessing methodology that permits testing of rotated scans. Prior to these results, the images could not have been properly rotated in MATLAB as their matrices were not square or 1:1. The results in this series of tests provided a powerful update to the preprocessing of the scans. Instead of losing data in future images by cropping them to match other ones, their aspect ratios can be reduced. The visual assumption that no significant data was lost in the aspect ratio modifications was supported by the continuation of 100% classification accuracy or complete misclassification of all the defective data sets. Finally, by proving the efficacy of reducing the aspect ratios, the artificial creation of defects using preexisting data by rotation was made viable.

### **3.4 Investigation of Rotating Images**

Following the positive results in the testing of scans with modified ratios, experimentation on the model's ability to predict rotated samples was performed. First, the model was trained using a

baseline sample set identical to that used in the resizing experiments and with a regularization penalty of 1. It is important to note that this sample set did not include any rotated samples. Following the training of the network, a brand-new sample set was uploaded that included varying rotated data inputted to the neural network using the prior weights. The motivation behind rotating the scans is to move the defect data to new locations within the matrix and simulate a different defective block of cellular glass. Figure 9 shows a comparison of a defective sample before and after it was rotated to illustrate how it simulates a unique defective block.



**Figure 9. Artificial Defect Sample by Rotation**

The testing using rotated samples was held to 200 samples, as previous results showed zero effect on the model's accuracy when larger samples were used. Instead, the rotation amounts were varied along with having multiple sets of samples rotated in differing amounts. Ultimately, the model maintained 100% accuracy throughout all iterations of the test which are reported in Table 4.

**Table 4. Rotation Results**

<b>TEST METHOD</b>	<b>REPORTED ACCURACY (PREDICTION = LABEL)</b>
90 deg of rotation	<i>100%</i>
180 deg of rotation	<i>100%</i>
Combined 90 and 180 def of rotation	<i>100%</i>

The final test performed to find a model failure was incorporating regularization tests to the training data and then retesting the same three configurations of rotated images. The training of the neural network would continue to use an unrotated test set composed of 10 defective and 190 healthy samples and now include varying penalty values for regularization. A new sample of rotated images was then inputted into the neural network in the same manner as the prior tests.

**Table 5. Regularization Testing with Rotated Images**

<b>TEST METHOD</b>	<b>REPORTED ACCURACY (PREDICTION = LABEL)</b>
<b>Lambda = 5</b>	
Combined 90 and 180 deg of rotation	<i>95%</i>
<b>Lambda = 2.5</b>	
Combined 90 and 180 deg of rotation	<i>95%</i>
<b>Lamba = 1.5</b>	
Combined 90 and 180 deg of rotation	<i>97.5%</i>
<b>Lambda = 1.37</b>	
Combined 90 and 180 deg of rotation	<i>100%</i>
<b>Lambda = 1.25</b>	
Combined 90 and 180 deg of rotation	<i>100%</i>

Table 5 reports the results of the iterative tests along with their respective lambda values. The results showed the model would become overgeneralized and misclassify all the defective samples as healthy when a regularization value as low as 2.5 was used. This was significantly lower than the lambda that caused this type of generalization when rotation was not completed. A lower level of regularization signals that rotating the images was successful in introducing more variety to defective samples. Additionally, when the model was trained using 1.5 as the regularization penalty half of the defective samples were misclassified. This was the only testing iteration to produce varying hypotheses for defective samples. All of the prior tests resulted in either fully accurate classification or complete misclassification of defects. However, once the images that were misclassified in the test were further inspected, they were revealed to all be rotated the same amount of 180 degrees.

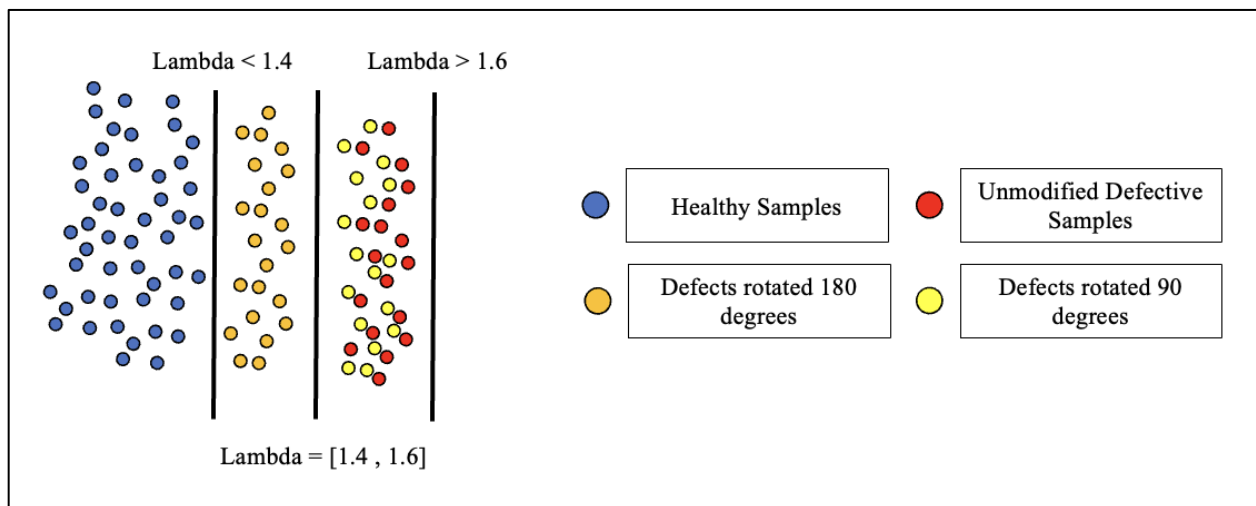


**Figure 10. Idealized Illustration of the Model Applied to Rotated Scans**

Fig 10 illustrates how the rotated data and the model fit resulted in the isolated misclassification of the defective samples that were rotated 180 degrees, but not those rotated 90 degrees. Note the

figure is not representative of the true model and distribution. Rather, the figure serves as an idealized visual to illustrate the issue was underfitting.

When the model misclassifies all of a certain type of defect (180 deg in this test) it is an issue of underfitting—not that it cannot classify the dataset at all, which is evident by slightly lower lambda resulting in 100% accuracy. Consequently, the misclassification by the model was determined to be caused by overgeneralization for those specific samples rather than a more terminal issue. In conclusion, the neural network proved to be applicable across a range of sample types and flawless in classification.

### **3.5 Summary of Results**

The computational results of the testing on the design of the regularized neural network indicate it is a strong, reliable, and accurate method of defect identification and classification of cellular glass samples. The testing of the initial parameters revealed that the model performed as anticipated. In that testing, insight was gained into the statistical distribution of defective and healthy samples. In the narrow data set, both sample types were deemed to be mutually exclusive. These results fueled further investigations on larger sample sizes (3.2) and new defect types (3.3 – 3.4 ) to increase the variety of defective samples. The motivation of these investigations was to observe the misclassification of only a portion of defective samples rather than the all or none results seen in 3.1. The testing of larger sample sizes failed to produce the failure characteristic aimed for; instead, it further supported the theory of mutual exclusivity of defective and healthy samples. Finally, the artificial creation of new defects was explored by first reducing the aspect ratios of each sample to 1:1 followed by rotations. The 100% accuracy observed in the aspect ratio experiments provides two important developments: 1. the cropping of the scans in the preprocessing step could be replaced with an improved method, and 2. rotating existing defective samples

was made possible with each scan now stored in a square matrix. The rotation trial results continued to support that all available defective samples were statically significant for healthy ones. The testing in this research concluded that the neural network design succeeded at the goal of identifying defective from healthy samples of cellular glass using CT scans.

## Chapter 4

### Conclusions

Cellular glass is an insulation material applied in an array of projects because of its high compressive strength-to-weight ratio and low thermal conductivity. Existing research has proven that the density profile of a sample of cellular glass drives those material properties across a large range: 1.5 – 5 MPa. Currently, manufacturers lack a process for defect identification and classification of cellular glass products.

This research set out to establish a regularized neural network capable of identifying defective samples of cellular glass from healthy ones. Experiments were conducted on the neural network using CT scans of one defective sample and a separate healthy one. The testing included baseline tuning of the model, expansion of the sample size, and artificial creation of new defective samples. It concluded that the model was highly accurate at separating the defects. However, a major limitation of this research was the lack of availability of additional defective samples. The defective scans were manipulated through various rotations in an attempt to increase variation. However, the only misclassification observed across the array of tests was caused by regularization, causing the model to underfit the data.

Future research should investigate the inclusion of a larger pool of defective and healthy samples. This would result in improved comprehension of the regularization requirements for a full-scale application. As previously stated, the material properties of cellular glass vary across a large range and are driven by the density profile of a given sample. Therefore, expanding the labels to cover the range of material properties rather than only defective or healthy should be tested. Finally, testing of the sample block before and after defects are created should be

performed. A limitation in this research was the lack of access to healthy and defective scans with minimal differences other than the defects. Instead, the samples used were different sizes which could have increased the model's ability to detect them from one another.

**BIBLIOGRAPHY**

- [1] C. P. SMOLENSKI Mgr, "Cellular Glass Foams," Pittsburgh, 1984.
- [2] R. W. Gerrish, "D-2 Cellular Glass Insulation For Load-Bearing Application In Me Storage Of Cryogenic Fluids," *Adv Cryogenic Engineering*, pp. 242–250, 1977.
- [3] A. G. Ryan, S. Kolzenburg, A. Vona, M. J. Heap, J. K. Russell, and S. Badger, "A proxy for magmatic foams: FOAMGLAS®, a closed-cell glass insulation," *Journal of Non-Crystalline Solids: X*, vol. 1, Mar. 2019.
- [4] M. Osfouri and A. Simon, "Study on the thermal conductivity and density of foam glass," *Pollack Periodica*, Nov. 2022.
- [5] P. M. Gammell and M. A. Adams, "Detection of Strength Limiting Defects in Cellular Glasses by Dielectric Measurements," *J Nondestr Eval*, vol. 2, no. 2, pp. 113–118, 1981.
- [6] B. Alramahi, "Applications of Computerized Tomography (CT) to Characterize the Internal Structure of Geomaterials: Limitations and Challenges," *American Society of Civil Engineers*, pp. 88–95, 2006.
- [7] Y. Nikishkov, L. Airoidi, and A. Makeev, "Measurement of voids in composites by X-ray Computed Tomography," *Compos Sci Technol*, vol. 89, pp. 89–97, Dec. 2013.
- [8] M. Goueygou, Z. Lafhaj, and F. Soltani, "Assessment of porosity of mortar using ultrasonic Rayleigh waves," *NDT and E International*, vol. 42, no. 5, pp. 353–360, Jul. 2009.
- [9] J. S. Popovics and K. V. L. Subramaniam, "Review of Ultrasonic Wave Reflection Applied to Early-Age Concrete and Cementitious Materials," *J Nondestr Eval*, vol. 34, no. 1, Mar. 2015.
- [10] T. M. Meksen, B. Boudraa, R. Draï, and M. Boudraa, "Automatic crack detection and characterization during ultrasonic inspection," *J Nondestr Eval*, vol. 29, no. 3, pp. 169–174, Sep. 2010.

- [11] M. Khanzadeh, S. Chowdhury, M. Marufuzzaman, M. A. Tschopp, and L. Bian, “Porosity prediction: Supervised-learning of thermal history for direct laser deposition,” *J Manuf Syst*, vol. 47, pp. 69–82, Apr. 2018.
- [12] S. Lee *et al.*, “A deep learning model for burn depth classification using ultrasound imaging,” *J Mech Behav Biomed Mater*, vol. 125, Jan. 2022.
- [13] R. Li, X. Gu, Y. Shen, K. Li, Z. Li, and Z. Zhang, “Smart and Rapid Design of Nanophotonic Structures by an Adaptive and Regularized Deep Neural Network,” *Nanomaterials*, vol. 12, no. 8, Apr. 2022.
- [14] Z. Waszczyszyn and L. Ziemia Nski, “Neural networks in mechanics of structures and materials ± new results and prospects of applications,” *Computers and Structures*, vol. 79, no. 1, pp. 2261–2276, 2001.
- [15] I. Sajedian, J. Kim, and J. Rho, “Finding the optical properties of plasmonic structures by image processing using a combination of convolutional neural networks and recurrent neural networks,” *Microsyst Nanoeng*, vol. 5, no. 1.
- [16] R. Li, X. Gu, Y. Shen, K. Li, Z. Li, and Z. Zhang, “Smart and Rapid Design of Nanophotonic Structures by an Adaptive and Regularized Deep Neural Network,” *Nanomaterials*, vol. 12, no. 8, Apr. 2022.
- [17] A. G. Ryan, S. Kolzenburg, A. Vona, M. J. Heap, J. K. Russell, and S. Badger, “A proxy for magmatic foams: FOAMGLAS®, a closed-cell glass insulation,” *Journal of Non-Crystalline Solids: X*, vol. 1, 2019.
- [18] “Standard Test Method for Thermal Conductivity, Thermal Diffusivity, and Volumetric Heat Capacity of Engine Coolants and Related Fluids by Transient Hot Wire Liquid Thermal Conductivity Method 1”.



## Appendix A

### Front End Code

```

%% Image Upload
testdata=zeros(200,3826600); % 200 defective + 10 healthy
% Defective sample upload
for iii= 1:10
[img,map] = imread(['Sample1_with_defects\Sample1_with_defects' num2str(iii,'%05.f)], 'tif');
    %[h, w, c] = size(img);
    %n_w = uint16(1900);
    %n_img = imresize(img, [h n_w]);
    % %r_img = rot90(n_img); %rotating images 90 deg
    %temp = r_img(:)
    %temp = n_img(:);
    temp = img(:);
    testdata(iii,:)=temp';
end
% Healthy Sample Upload
for jjj=1:190
[img,map] = imread(['Sample4\Sample4' num2str(jjj,'%05.f)], 'tif');
    % Aspect Ratio Processing
    %[h, w, c] = size(img);
    %n_w = uint16(1900);
    %n_h = uint16(1900);
    %n_img = imresize(img, [n_h n_w]);
    % %r_img = rot90(n_img); %rotating images 90 deg
    %temp = r_img(:)
    %temp = n_img(:);
    temp = img(100001:3926600);
    testdata(jjj+10,:)=temp';
end
%
```

```

X = testdata;
y = ones(200,1); % Defective Label
y(11:200,1) = 2; % Healthy Label

%% Preallocation
m = size(X);
input_layer_size = length(X); %Number of pixels in the scans
hidden_layer_size = 25;
num_labels = 2;

%% Random Initialization
initial_Theta1 = randInitializeWeights(input_layer_size, hidden_layer_size);
initial_Theta2 = randInitializeWeights(hidden_layer_size, num_labels);

%% Learning Parameters
% Unroll parameters
initial_nn_params = [initial_Theta1(:) ; initial_Theta2(:)];

tic
options = optimset('MaxIter', 40);
lambda = 30;

costFunction = @(p) nnCostFunction(p, input_layer_size, hidden_layer_size, num_labels, X, y,
lambda); % shorthand

% Now, costFunction is a function that takes in only one argument (the neural network
parameters)
[nn_params, ~] = fmincg(costFunction, initial_nn_params, options);

Theta1 = reshape(nn_params(1:hidden_layer_size * (input_layer_size + 1)), hidden_layer_size,
(input_layer_size + 1));

```

```

Theta2 = reshape(nn_params((1 + (hidden_layer_size * (input_layer_size + 1))):end), num_labels,
(hidden_layer_size + 1));
%% Prediction and Accuracy
% rp = randi(110);
pred = predict(Theta1, Theta2, X); %(predictor using a random image from the test data)
% fprintf('Neural Network Prediction: %d \n', pred)
fprintf('\nTraining Set Accuracy: %fn', mean(double(pred == y)) * 100);
toc

```

### Random Initialization Function

```

function W = randInitializeWeights(L_in, L_out)
%RANDINITIALIZEWEIGHTS Randomly initialize the weights of a layer with L_in
%incoming connections and L_out outgoing connections
% W = RANDINITIALIZEWEIGHTS(L_in, L_out) randomly initializes the weights
% of a layer with L_in incoming connections and L_out outgoing
% connections.

W = zeros(L_out, 1 + L_in);

eps_init = sqrt(6) / sqrt(L_in + L_out);
W = rand(L_out, 1+ L_in) * eps_init - eps_init;

```

### Neural Network Training Function

```

function [J grad] = nnCostFunction(nn_params,input_layer_size, hidden_layer_size, num_labels,
X, y, lambda)
% NN COSTFUNCTION Implements the neural network cost function for a two-layer
% neural network which performs classification
% [J grad] = NN COSTFUNCTION(nn_params, hidden_layer_size, num_labels, ...
% X, y, lambda) computes the cost and gradient of the neural network. The
% parameters for the neural network are "unrolled" into the vector

```

```

% nn_params and need to be converted back into the weight matrices.

% Reshape nn_params back into the parameters Theta1 and Theta2, the weight matrices
% for a 2-layer neural network
Theta1 = reshape(nn_params(1:hidden_layer_size * (input_layer_size + 1)), ...
                hidden_layer_size, (input_layer_size + 1));

Theta2 = reshape(nn_params((1 + (hidden_layer_size * (input_layer_size + 1))):end), ...
                num_labels, (hidden_layer_size + 1));

% Variable Set Up
m = size(X, 1);

J = 0;
Theta1_grad = zeros(size(Theta1));
Theta2_grad = zeros(size(Theta2));

% Part 1: Feedforward the neural network and return the cost in the
%       variable J. After implementing Part 1, you can verify that your
%       cost function computation is correct by verifying the cost
%       computed in ex4.m
%
% Part 2: Implement the backpropagation algorithm to compute the gradients
%       Theta1_grad and Theta2_grad. You should return the partial derivatives of
%       the cost function with respect to Theta1 and Theta2 in Theta1_grad and
%       Theta2_grad, respectively. After implementing Part 2, you can check
%       that your implementation is correct by running checkNNGradients
%
% Part 3: Implement regularization with the cost function and gradients.

%% Cost Function (feed forward and implementing the cost function)
X = [ones(m,1), X];

```

```

a1 = X;
z2 = a1*Theta1';
a2 = sigmoid(z2);
a2 = [ones(size(a2,1),1), a2];
z3 = a2*Theta2';
a3 = sigmoid(z3);
H_x = a3;

y_vec = (1:num_labels)==y;
J = 1/m * (sum(sum(-y_vec.*log(H_x) - (1-y_vec).*log(1-H_x))));

%% Backpropogation to find grad_1 and grad_2

del3 = a3 - y_vec;
del2 = (del3*Theta2) .* [ones(size(z2,1),1) sigmoidGradient(z2)];
del2 = del2(:,2:end);

%DELTA3 = A3 - y_Vec;
%DELTA2 = (DELTA3 * Theta2) .* [ones(size(Z2,1),1) sigmoidGradient(Z2)];
%DELTA2 = DELTA2(:,2:end);

Theta1_grad = (1/m) * (del2' * a1);
Theta2_grad = (1/m) * (del3' * a2);

%% Regularization
J = J + (lambda/(2*m)) * (sum(sum(Theta1(:,2:end).^2)) + sum(sum(Theta2(:,2:end).^2)));

Theta1_grad = Theta1_grad + (lambda/m)* [zeros(size(Theta1,1),1) Theta1(:,2:end)];

Theta2_grad = Theta2_grad + (lambda/m)* [zeros(size(Theta2,1),1) Theta2(:,2:end)];

% Unroll gradients

```

```
grad = [Theta1_grad(:) ; Theta2_grad(:)];  
end  
end
```

### Predict Function

```
function p = predict(Theta1, Theta2, X)  
%PREDICT the label of an input given a trained neural network  
% p = PREDICT(Theta1, Theta2, X) outputs the predicted label of X given the  
% trained weights of a neural network (Theta1, Theta2)  
  
% Useful values  
m = size(X, 1);  
num_labels = size(Theta2, 1);  
  
p = zeros(size(X, 1), 1);  
  
h1 = sigmoid([ones(m, 1) X] * Theta1');  
h2 = sigmoid([ones(m, 1) h1] * Theta2');  
[dummy, p] = max(h2, [], 2);  
  
end
```

## ACADEMIC VITA

# BENJAMIN BURLOVIC

412.855.0367 | burlovicb@gmail.com | Pittsburgh, PA

### EDUCATION

---

**The Pennsylvania State University | Schreyer Honors College**  
*College of Engineering* | Bachelor of Science in Mechanical Engineering  
*College of the Liberal Arts* | Bachelor of Science in Economics

**University Park, PA**  
*Class of May 2023*

### PROFESSIONAL EXPERIENCE

---

#### **McKinsey & Company**

*Incoming Business Analyst*

**Pittsburgh, PA**  
*Sep 2023*

#### **Laboratory of Sound and Vibrations Research**

*Undergraduate Researcher*

**University Park, PA**  
*Jan 2022 – Present*

- Writing an image classification neural network to be used in conjunction with ultrasound imagery on the manufacturing line for live defect detection of foam glass products
- Documenting the research done to determine how to feature the image data in MATLAB and other applications of ultrasound image classification in the form of an honors thesis

#### **Deloitte**

*Summer Strategy Scholar*

**New York, NY**  
*Jun 2022 – Aug 2022*

- Supported my team across three varying workstreams by taking meeting notes, creating slide decks, performing Excel analyses, and communicating with our project stakeholders
- Strengthened my knowledge of Deloitte Consulting's operation model by joining firm initiatives, reviewing previous proposals, and interviewing consultants in a variety of offerings

#### **KCF Technologies**

*Product Strategy Intern*

**State College, PA**  
*Jun 2021 – Aug 2021*

- Analyzed vibrational data from Ford Automotive assets to increase the asset's lifespan in a potential decrease of 100 hours of downtime equating to approximately \$700,000 in savings
- Developed a business case outlining multiple areas in which KCFs software could be updated and improved to allow for faster analysis by engineers allowing for further growth of the company

### LEADERSHIP AND INVOLVEMENT

---

#### **Schreyer Consulting Group**

*President | VP of Alumni Relations | Chair of Student Engagement*

**University Park, PA**  
*Sep 2019 – Present*

- Reignited the organization's efforts to host alumni speakers and information sessions to help educate first and second-year Schreyer students interested in exploring various consulting roles

#### **Alpha Kappa Psi Co-ed Professional Business Fraternity**

*Fraternity Educator | New Member Education | Recruitment Chair | Pledge Class President*

**University Park, PA**  
*Jan 2020 – Present*

- Hosted bi-weekly meetings with the newest members of the club to help expedite their learning process of the club's most important events and their responsibilities as members
- Planned and executed a marketing campaign and various recruitment events that led to the club receiving over 100 applicants and ultimately had 100% offer acceptance

### HONORS, SKILLS, AND ACTIVITIES

---

**Honors:** Academic Excellence Scholarship, Winner of the National Deloitte Case Competition, Dean's List (7/7), Chapel Executive Intern, 2022–2023 College of the Liberal Arts Undergraduate Studies Scholarship

**Skills:** Established in SolidWorks, MATLAB, Java, Excel, PowerPoint; Bosnian/Croatian/Serbian (Native speaker)

**Activities:** Schreyer Scholar Assistant, Economics Grader (5 semesters), Traveling to the Mediterranean, Skiing